Hindawi
Journal of Chemistry
Volume 2019, Article ID 3241061, 18 pages
https://doi.org/10.1155/2019/3241061

Research Article

Transition Metal Complexes of Mixed Bioligands: Synthesis, Characterization, DFT Modeling, and Applications

Mohamed S. A. Abdel-Mottaleb[1] **and Eman H. Ismail**[2]

[1]*Nano-Photochemistry Solarchemistry and Computational Chemistry Labs, Chemistry Department, Faculty of Science, Ain Shams University, Abbassia, 11566 Cairo, Egypt*
[2]*Analytical and Inorganic Chemistry Labs, Chemistry Department, Faculty of Science, Ain Shams University, Abbassia, 11566 Cairo, Egypt*

Correspondence should be addressed to Mohamed S. A. Abdel-Mottaleb; phochem08@photoenergy.org

Received 3 April 2019; Accepted 28 April 2019; Published 23 May 2019

Academic Editor: Hassan Arida

Divalent transition metal complexes [MGlu-Arg $(H_2O)]H_2O$ and [MGlu-Arg $(H_2O)]H_2O$, where M = Co, Ni, Cu, and Zn, Glu = glutamic acid, and Arg = L-arginine, are prepared and characterized using different techniques. DFT and TD-DFT modelling validated and interpreted some experimental results. Weight loss technique reveals efficient corrosion inhibition action of these complexes towards aluminum metal at different temperatures. Our results point to corrosion inhibition through chemical adsorption on the aluminum surface. Additionally, a facile calcination of Co and Cu complexes at 550°C yields nanosized oxides of Co_3O_4, CoO, and CuO crystalline phases. The complexes show remarkable biological activities towards pathogenic bacteria and fungi. Moreover, in vitro anticancer activity evaluation of these complexes is achieved against hepatocellular carcinoma (HepG-2). The results are correlated with molecular descriptors such as chemical potential and hardness obtained from the frontier orbitals.

1. Introduction

The chemistry of amino acid coordination compounds has always been an intriguing challenge to the inorganic chemists. This class of molecules have been found throughout the life science and vary tremendously in their function and complexity. These compounds play an essential part of metabolism and cellular signaling and as a part of drugs and as hydrogen storage media [1].

Many transition metals with mixed amino acid complexes revealed their biological activity, which place them in several biochemical processes [2–5]. The ternary complex models provide information about how biological systems achieve their specificity and stability, as well as strategies, to improve these features for biotechnological applications [6].

Glutamic acid (Glu) (2-Aminoglutamic) is one of the 20 most common natural amino acids, which is considered to be one of the building blocks in protein synthesis [7–9]. It is of interest for brain/memory and biochemistry and as anticancer drug by reducing its toxicity against normal cells [10]. Glutamic acid has three potential coordination sites: the amino nitrogen and two carboxylic groups, and the electronegativity of the N and O atoms as well as the flexible skeleton of the glutamic facilitate its coordination behavior as bidentate or tridentate ligand [11].

Arginine is an essential amino acid that is physiologically active in the L-form. L-arginine appears as a zwitter ion with a protonated guanidine group in aqueous solutions, a spontaneous process resulting in a thermodynamically durable form in both solutions and crystals. The presence of a guanidine group in L-arginine enhanced the interesting behavior of antimicrobial activity against bacteria and fungi [12]. The coordination mood for a copper complex with amino acids like L-arginine and glutamic acid is bound by an amino nitrogen and a carboxyl oxygen [13].

We focus here on the preparation and characterization of this class of mixed amino acid complexes of four divalent transition metal ions of Co, Ni, Cu, and Zn.

Modelling using DFT theory and TD-DFT will be investigated in an attempt to validate and characterize structural and electronic properties of M(II) Glu-Arg complexes in aqueous solution. This will shed light on the nature of M-L interaction. Such knowledge is likely to provide some help in the rational design of new complexes of biological importance. Additionally, cytotoxicity will be evaluated. Investigation of the biological activities include g-negative (*P. aeruginosa* and *E. coli*) pathogenic bacteria and g-positive (*Streptococcus* p. and Bacillis sub.) pathogenic bacteria.

It is known that amino acids act as an eco-friendly inhibitor for several metals as copper, aluminum, steel, and nickel. L-arginine and its zinc complex are used as nontoxic and low-cost corrosion inhibitors for carbon steel [14–16]. Thus, we will undertake corrosion inhibition abilities studies of the complexes prepared towards aluminum because they are widely exploited in automobile, aerospace, and household industries.

Additionally, the metal complexes could be considered as a precursor for thermal preparation of nanosized metal oxides. Thus, we will investigate calcinating the complexes under investigations to check the possibility of obtaining metal nano-oxides in a facile way for possible application as photocatalysts.

2. Experimental

2.1. Materials and Preparation of the Complexes. All chemicals were purchased from Sigma-Aldrich. Glutamic acid (CAS Number: 56-86-0) and L-arginine (CAS Number: 74-79-3) ligands, as well as metal carbonates $CoCO_3{\cdot}3Co(OH)_2$ (CAS Number: 12602-23-2), $NiCO_3{\cdot}2Ni(OH)_2{\cdot}4H_2O$ (CAS Number: 12607-70-4), $CuCO_3{\cdot}Cu(OH)_2{\cdot}H_2O$ (CAS Number: 12069-69-1), and $2ZnCO_3{\cdot}3Zn(OH)_2$ (CAS Number: 5263-02-5), were used without further purifications.

[M(II)(Glu)(Arg)] complexes were synthesized following the method used in [16]. Refluxing equal-molar amounts of M(II)carbonate (1 mmol, powder) and water-soluble glutamic acid (1 mmol), L-arginine (1 mmol) in ~100 ml bidistilled water at about 80–363 K for 2–3 days gives dense precipitate upon scratching. The obtained dense precipitate was filtrated and washed with absolute ethanol. Crystallization of the new ternary complexes was achieved in absolute ethanol/bidistilled water mixed solvent. Unfortunately, no single crystals could be obtained.

2.2. Instrumentation. The contents of C, H, and N were determined by Vario El Elementar, while metal percentages were determined by atomic absorption spectrometry (PerkinElmer AAs 3100) FTIR spectra of the ligands, and the complexes in KBr discs were recorded on a Jasco FTIR-300E Spectrometer (400–4000 cm^{-1} range), microanalytical laboratory, in the central laboratory of Ain Shams University.

Mass spectra were recorded at 350C° and 70 eV on Shimadzu GC/MS-QP5050A spectrometer, and ESR spectrum of the Cu complex was recorded at room temperature using a Bruker ESR-spectrometer model EMX at 9.706 GHz (X-band) using 2,2-diphenylpyridylhydrazone (DPPH) as standard ($g = 2.0037$).

Conductivity measurements of 10^{-3} M aqueous solutions (de-ionized water) at 25°C were carried out using WTW D-812 Weilheim conductivity meter, model LBR, fitted with a cell model LTA 100.

2.3. Thermogravimetric Analysis. Thermogravimetric analysis (TGA) of metal complexes was carried out starting from room temperature ~303 K to 1273 K under nitrogen atmosphere at a heating rate 283 $K{\cdot}min^{-1}$ using TA instrument, model SDT600. Mass spec., ESR, and TGA analysis were done in National Research Center lab, Cairo. The UV-Vis spectra were recorded in aqueous solutions (10^{-2} M) at room temperature with typical ranges from 800 to 190 nm on Cary 100 which is done in the microanalytical laboratory, in the central laboratory of Ain Shams University.

2.4. Nanosized Metal Oxide Preparation. The metal complexes were calcined at 550°C for 6 h, and the metal oxides obtained were characterized by X-ray diffraction, scanning electron microscopy, and transmission electron microscopy. XRD analysis showed that the obtained oxides are crystalline and corresponded to the Co_3O_4, CoO, and CuO phases. Crystal size and shape were determined by SEM.

2.5. Magnetic Susceptibilities. Magnetic susceptibilities were measured at room temperature by the Gouy method using a magnetic susceptibility balance Johnson Matthey, Alfa products, model MKI. Diamagnetic corrections were calculated from PASCAL's constants. Mercury tetrakis-thiocyanatocobaltate was used as a standard. The analysis was carried out in microanalytical laboratory, Cairo University.

2.6. Corrosion Inhibition Materials and Methods. A pure aluminum foil sheet (Al) of 98.92% purity which is press-cut to form specimens with dimensions of 1 cm × 1 cm × 0.15 cm was used.

One liter of 1 M HCl solution was prepared using deionized water. Al samples were immersed for 7 hours in 20 ml of 1M HCl used as corrosive solution. An electronic weighing balance (Easyway-JA 1003A), micrometer heating mantle, and a water bath were used. Various concentrations (10^{-2}–10^{-5} M) of mixed ligands (glutamic acid + arginine by the ratio 1 : 1) and their ternary metal complexes were prepared and dissolved in 1 M HCl and examined as inhibitors for Al corrosion by weight loss method. The mixed ratio (1 : 1) of these two ligands was the same ratio as that used in preparation of the four metal complexes. Before each run, the surface of Al was polished with different grades of emery papers, degreased with ethyl alcohol, washed thoroughly with double distilled water, dried in air and finally weighed. Then these specimens were immersed in 20 ml inhibited and uninhibited 1 M HCl solution in open containers for 7 h for aluminum specimens as immersion time

then, they were withdrawn from the test solution, washed with deionized water and acetone, dried, and reweighed. The container was placed in a water bath maintained at (303 ± 1) K. The experiments were operated without (blank) and with the various concentrations of the mixed ligands and the complexes separately. The weight loss was taken as the difference in weight of the specimen before and after the immersion time. The experiments were carried out in water bath with temperature range 293–313 ± 1 K.

2.7. Biological Activity. The antimicrobial activity of the prepared ternary metal complexes against two gram-positive bacteria (*Streptococcus pneumoniae*, *Bacillis subtilis*), two gram-negative bacteria (*Pseudomonas aeruginosa*, *Escherichia coli*), and four fungi (*Aspergillus fumigates*, *Syncephalastrum racemosum*, *Geotricum candidum*, *Candida albicans*) were investigated by a Regional Center for Mycology and Biotechnology (RCMB), Al-Azhar University, Cairo.

2.8. Cytotoxicity. Cytotoxicity evaluation using viability assays was performed by a Regional Center for Mycology & Biotechnology (RCMB), Al-Azhar University Cairo. The inhibitory activity of ternary metal complexes is screened against the cell line hepatocellular carcinoma (HepG-2).

2.9. Computational Methods. Density functional theory (DFT) and its time-dependent extension (TD-DFT) theory, employing BP86D3/DEF2-SVP model, and auxiliary basis DEF2/JK were carried out using Orca 4.0.1.2 package [17]. Our calculation utilizes the atom-pairwise dispersion correction with the Becke–Johnson damping scheme (D3BJ) [18, 19]. RI approximation [20] was used. Overlap-fitted RIJCOSX approximation was also utilized as a speed-up option leading to enhanced speedups [21, 22] with almost no loss of accuracy [23]. First, we ran a geometry optimization and frequency job using BP86D3/DEF2-SVP) and auxiliary basis def2/J [18, 19]. All frequency modes are real indicating that the equilibrium geometry is reached. We used the same model for EPR simulations of the doublet state. In the case of UV-Vis computations, we utilized different models including CAM-B3LYP functional without returning a satisfactory result matching the experimental results. The most successful one that produced result in excellent agreement with the experiment was BP86D3/DEF2-SVP [18–20] and utilizing def2/J auxiliary basis. We utilized SMD solvation model [24]. Spartan 16 parallel package (https://www.wavefun.com/) has been used to obtain the potential energy surfaces (PESs) at the ωB97X-D/6-31G(*D*) level of the DFT.

A Broadberry workstation (40 cores) (UK) and a Mac Pro (12 core) workstation were used.

3. Results and Discussion

3.1. Structure and Spectroscopic Properties. Elemental analyses (C, H, N, and metal) and physical and chemical properties of the prepared ternary complexes are given in Table 1, where **(1)**, [Co·Glu·Arg·$(H_2O)2]\cdot 0.5H_2O$; **(2)**, [Ni·Glu·Arg·$(H_2O)_2]\cdot 0.5H_2O$; **(3)**, [Cu·Glu·Arg]·H_2O; and **(4)**, [Zn·Glu·Arg·$(H_2O)2]\cdot H_2O$.

The thermal decomposition of these complexes in the range (511–603 K) indicates thermal stability. The effervescence test with sodium carbonate confirmed that all the prepared complexes are containing free acidic proton. The magnetic moments, molecular weight (Mol. wt.), and molar conductivity values are given in Table 1. The pH values indicate slightly acidic character. The obtained experimental and theoretical data confirm the suggested structures shown in Figures 1 and 2.

The paucity of information about mixed amino acids (glutamic acid and arginine) metal complexes motivated us to investigate their molecular structures using DFT theory to characterize structural and electronic properties considering Co(II) and Cu(II) Glu-Arg complexes in aqueous solution as representative of all complexes. Optimized geometries are depicted in Figure 1. Such knowledge is likely to provide some help in the rational design of new complexes for their biological importance.

In this pH range, glutamic acid and L-arginine are predominantly present in their zwitter ion form, and each has two coordination sites (one N and one COO^-), which are agreed with their distribution coefficients [24]. The analysis and optimized geometry computations suggested that Ni, the important vibrational frequencies of arginine, glutamic acid and their ternary metal complexes bands, (II) and Zn(II) complexes are of distorted octahedral structure similar to Co(II) complexes. Based on $10D_q$ values of these ternary complexes, the distorted octahedral structure is suggested for nickel, cobalt, and zinc complexes and square planar for copper complex. Moderate conductivity measured confirms the existence of intramolecular hydrogen bonds. Also, magnetic moments of the synthesized complexes have been measured in order to confirm their structures. The data are presented in Table 1.

3.1.1. IR Spectra. The important vibrational wavenumbers of arginine, glutamic, and their ternary metal complexes bands are listed in Tables 2 and 3. Arginine showed bands at 1698 and 1409 cm^{-1} assigned for asymmetric and symmetric stretching vibrations of the carboxylate moiety. It also showed medium broadband at 3086 cm^{-1} which attributed to the amino NH_2 group. The IR spectra of the complexes did not show any free carboxylic beaks due to strong intramolecular hydrogen bonding. Also, IR spectra of the four complexes exhibit crowded region between 3500 and 3000 cm^{-1}, where H_2O, –OH, and –NH stretching modes are expected to absorb. The broadband in the range 3300–3400 cm^{-1} could be attributed to the intramolecular hydrogen bonding (O…H–O, O…H–N, O–H…N). An example of the IR spectrum is given in Figure 1S. Similarly, glutamic acid IR spectra (Figure 3S) showed two bands at 1641, 1418, and 3062 cm^{-1} as reported before [25, 26].

Upon complexation, the NH stretching wavenumber is shifted to 3141–3184 cm^{-1}, indicating that the amino nitrogen groups are coordinated to the metal atom [27].

Table 1: Some experimentally observed and determined characteristics of the prepared complexes (found values between parentheses).

Complex	*C* (%)	*H* (%)	*N* (%)	Metal (%)	Color	Magnetic moment (Debye)	Decomp temp. (°C)	pH	Conductivity (mS)	Mol. (wt.)
(1)	31.0 (31.9)	5.9 (5.2)	16.5 (15.9)	13.9 (14.0)	Pink	4.13	290	5.6	3.480	425.3
(2)	31.1 (32.1)	5.4 (4.9)	16.5 (15.9)	13.8 (14.2)	Green	3.10	290	5.1	3.700	425.0
(3)	32.8 (32.1)	5.7 (6.2)	17.4 (17.8)	15.8 (16.4)	Blue	1.78	238	4.9	4.607	402.9
(4)	29.9 (30.4)	5.2 (4.8)	15.9 (15.3)	14.8 (15.1)	White	Diam.	330	5.3	3.557	440.7

(1) = [Co·Glu·Arg·$(H_2O)_2$]·0.5H_2O; **(2)** = [Ni·Glu·Arg·$(H_2O)_2$]·0.5H_2O; **(3)** = [Cu·Glu·Arg]·H_2O; **(4)** = [Zn·Glu·Arg·$(H_2O)_2$]·H_2O.

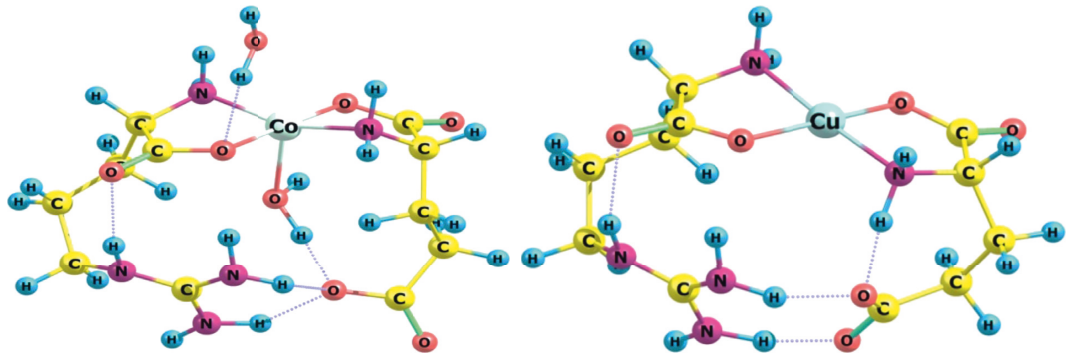

Figure 1: The optimized structure of Co(II) and Cu(II) complexes (dotted lines represent H bonding) indicating the coordination sites of the ligands, which result in the most stable orientation. Ni and Zn complexes have geometries similar to Co complexes.

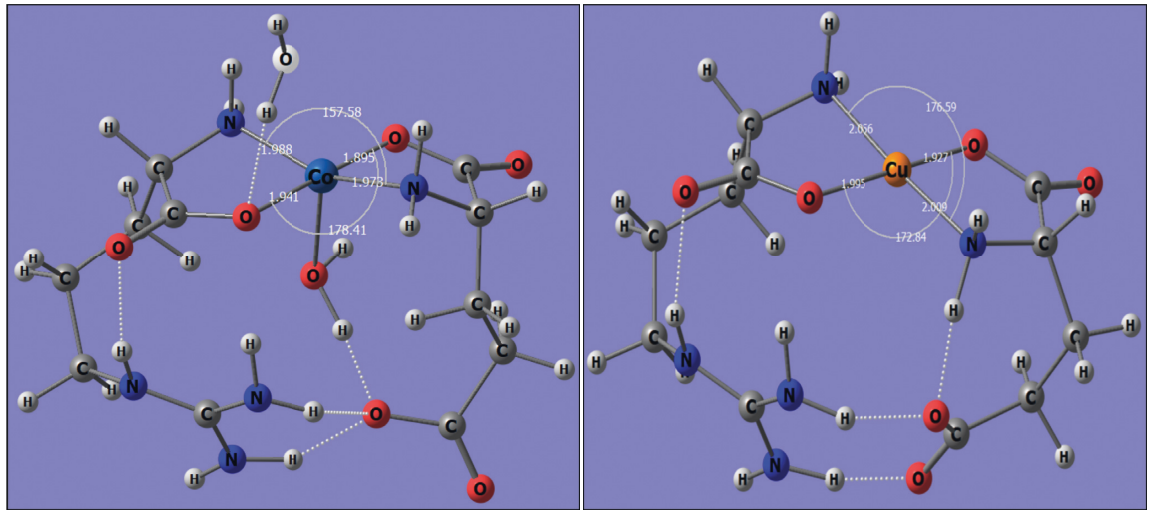

Figure 2: Optimized geometry around the central transition metal ions showing different bond lengths and angle.

Table 2: Experimentally and theoretically simulated IR spectra (in cm^{-1}) of the studied complexes. Assignment of experimentally measured IR key modes.

Ligands and complexes	υ (OH)	υ (NH)	υ (CN)	υ (COO_{asy})	υ (COO_{sy})	υ (M-O)	υ (M-N)
Glutamic	—	3062	1242	$1634_{(vs)}$	$1418_{(s)}$	—	—
Arginine	—	3087	1175 1586 1608	$1680_{(vs)}$	$1574_{(s)}$	—	—
[Co(glu)(arg)$(H_2O)_2$]·0.5H_2O	$3345_{(s)}$	3172	1131 1584 1609	$1663_{(s)}$	$1421_{(vs)}$	538	416

Table 2: Continued.

Ligands and complexes	υ (OH)	υ (NH)	υ (CN)	υ (COO_{asy})	υ (COO_{sy})	υ (M-O)	υ (M-N)
$[Ni(glu)(arg)(H_2O)_2]\cdot 0.5H_2O$	$3340_{(s,br)}$	3184	1122 1586 1607	$1658_{(s)}$	$1426_{(vs)}$	540	421
$[Cu(glu)((arg)]\cdot H_2O$	$3453_{(s)}$	3141	1126 1588 1604	$1676_{(s)}$	$1456_{(m)}$	572	456
$[Zn(glu)(arg)(H_2O)_2]\cdot H_2O$	$3427_{(s)}$	3144	1127 1582 1606	$1671_{(s)}$	$1425_{(s)}$	538	412

Table 3: Experimentally and theoretically simulated IR spectra (in cm^{-1}) of the studied complexes. Assignment of theoretically calculated IR key modes for Co(II) and Cu(II) complexes in the gas phase. Excellent match between experimentally determined and theoretically computed IR modes in case of Ni and Zn complexes is obtained.

Complex	υ (OH)	υ (COO)	υ (M-O)	υ (M-N)
$[Co(glu)(arg)(H_2O)_2]\cdot H_2O$	2513 (H-bonded H_2O and O of COO of Gu) 3521	1684.8 (Ar) 1740 (Gu)	554.3	463.6
$[Cu(glu)((arg)]H_2O$	3656 (caged H_2O) —	1677.8 (Gu) 1709.9 (Ar)	537.6	438.5

The C-NH_2 stretching bands of the guanidyl group of alpha amino group have shifted from 1242 to 1175 cm^{-1} of glutamic acid and L-arginine with respect into (1122–1131) cm^{-1} of the prepared metal complexes. In opposite situation, arginine has been shown to have two bands observed at 1586 and 1608 cm^{-1} due to the asymmetrical vibrations of the C-NH_2 bonds of the guanidino group, which is protonated to give the guanidinium form without a significant change in case of complexation [28].

The asymmetrical (υCOO_{asy}) and symmetrical (υCOO_{sy}) carboxylic groups are shifted in the prepared complexes to higher or lower values than their values in ligands case as shown in Tables 2 and 3, and also the difference between these bands are more than 200 cm^{-1} in all the prepared metal complexes which indicated that the deprotonated carboxylic groups in both ligands act as mono dentate groups.

All the prepared complexes exhibited bands in the range of 3340–3472 cm^{-1} of υ(OH) signifying that H_2O molecules exist in these complexes [29, 30].

The new confirmed bands only appear in the four prepared complexes at 538–572 cm^{-1} and 412–456 cm^{-1}, which are assigned to υ(M-O) and υ(M-N) stretching bands, respectively [31].

The optimized geometry of the complexes shows distorted overall octahedral (or better the square pyramidal C_{4v}-local symmetry of Co(II) ion) for the Co(II) complex and the slightly distorted square planar coordination of the Cu(II) ion in the Cu(II) complex. Ni and Zn complexes are of similar geometry to the Co complexes. Figure 3 shows that the local symmetry of both centrosymmetric cations is noticeably distorted with different M(II)-O and M(II)-N bond lengths and bond angles indicated in Figure 2.

The simulated PES maps [32], which shed light on the binding sites of the complexes, are depicted in Figure 3. Inspection of Figure 3 shows that Co(II) complex exhibits larger positive potentials (299 kJ/mol) than Cu(II) complex, which bears enhanced negative potential than that on Co(II) complex (the difference between negative and positive potential energy limits, (Delta) PES = 24, and −9 kJ/mol for Co(II) and Cu(II) complexes, respectively). Thus, Cu(II) complex could act as nucleophile, whereas Co(II) complex is of enhanced electrophilic nature during interactions.

3.1.2. Mass Spectra. The mass spectra of the four complexes were recorded and provided good evidence and confirmation of the molecular weight of these complexes (molecular ion peaks (MIPs) are detected under severe experimental conditions [16], which results in of splitting of crystalline water) (Figure 2S shows the mass spectrum of Zn(II) complex as example).

3.1.3. UV-Vis Absorption Spectra. Figure 4 shows the theoretical and experimental UV-Vis spectra of Co(II) and Cu(II) as examples. The results confirm that 1, 2, and 4 complexes have almost tetragonal distorted octahedral structure (C_{4v}-local symmetry) with different distortion degrees, which is obvious from the wavenumber and $10D_q$ values of the complexes compared to their literature values [33]. Cu complex exhibits slightly distorted square planar shape. Table 4 shows electronic spectral data and ligand field parameters such as D_q, B (free ion), B (complex), and β using band-fitting equation [34, 35].

The value of Racah parameter B (free ion) is larger than that of B (complex) due to the covalence bonding of the complex. The value of β (nephelauxetic ratio) < 1 is calculated according to equation (1). $\beta < 1$, validating octahedral geometry [34, 35].

$$\beta = \frac{B(\text{free ion})}{B(\text{complex})}. \quad (1)$$

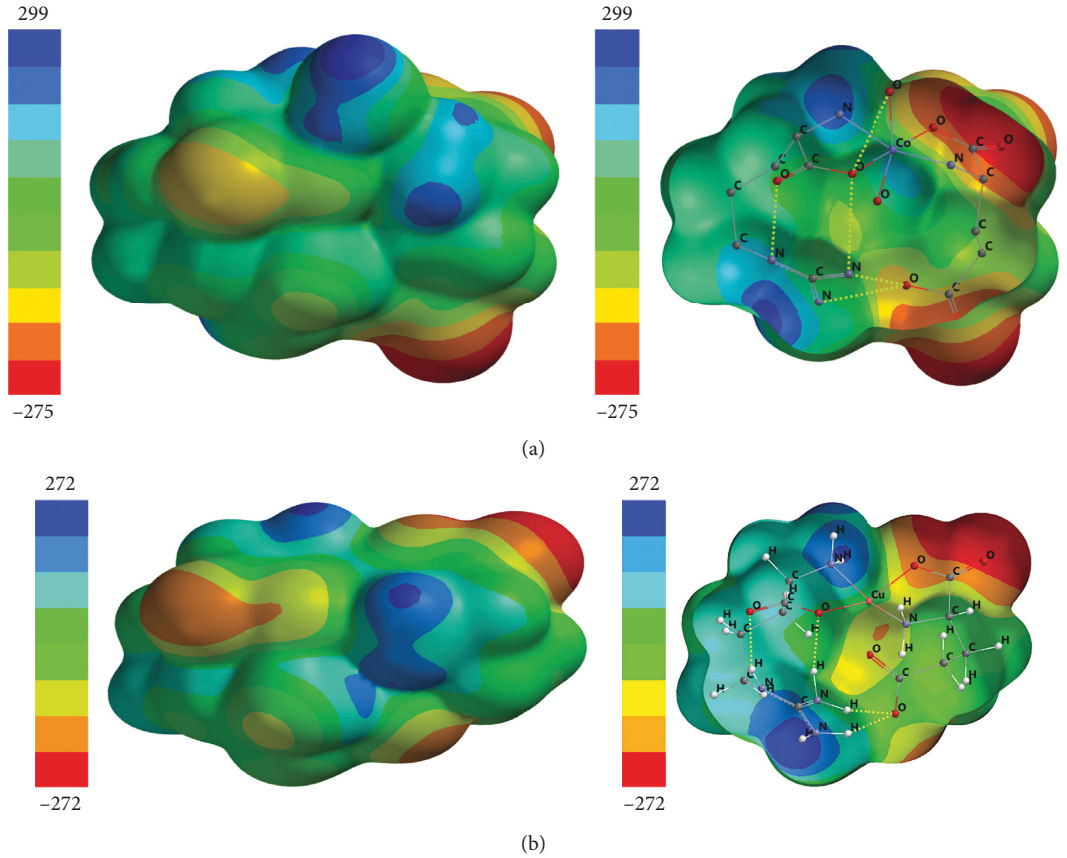

Figure 3: PES maps. (a) Co complex (upper pan: solid surfaces and lower pan: clipped surfaces) and legend color codes given in kJ/mol. (b) Cu complex (upper pan: solid surfaces and lower pan: clipped surfaces).

Spectral data and assignments are summarized in Table 4.

$10D_q$ for the nickel complex was determined by two procedures [34].

The first one is by solving equations (2) and (3) using the energy terms of the different triplet states transitions supplied for Ni(II) [34] as shown in Table 4:

$$\frac{E\left({}^3A_2 \longrightarrow {}^3T_2\right)}{E\left({}^3A_2 \longrightarrow {}^3T_1(F)\right)} = \frac{2\Delta/B}{15 + (3\Delta/B) - \left(225 - (18\Delta/B) + \left(\Delta^2/B^2\right)^{1/2}\right)}. \quad (2)$$

For Ni^{2+}, $B = 1080\ cm^{-1}$; thus,

$$\frac{E\left({}^3A_2 \longrightarrow {}^3T_2\right)}{E\left({}^3A_2 \longrightarrow {}^3T_1(F)\right)} = \frac{2\Delta/1080}{15 + (3\Delta/1080) - \left(225 - (18\Delta/1080) + \left(\Delta^2/1080^2\right)^{1/2}\right)},$$
$$\frac{15822}{25654} = \left(\frac{(2\Delta/B)}{\left(15 + (3\Delta/1080) - \left(225 - (18\Delta/1080) + \left(\Delta^2/1080^2\right)^{1/2}\right)\right)}\right). \quad (3)$$

Then, applying the trial and error procedure, a value for Δ that fits in equations (2) and (3) was found to be $10935\ cm^{-1}$, which suggested the octahedral structure. The second method for calculating $10D_q$ used Tanabe and Sugano diagrams for the different metal ion complexes. From Ni(II) diagram, we could be able to deduce the expected positions of the $({}^3A_{2g} \longrightarrow {}^3T_{2g})$ and the $({}^3A_{2g} \longrightarrow {}^3T_{1g})$ transitions. This method corresponds to a pure crystal field approach and assumes that the value of the free ion Racah parameter (B) is maintained in the complex.

Applying this procedure and considering the ratio of $\nu_1/\nu_2 = 15822/25641 = 0.62$, the best vertical line, which fulfils this ratio cuts the Δ/B axis at a value of 13.9 and $B_{complex}$, is calculated by equation (4). We found the value $765.273\ cm^{-1}$.

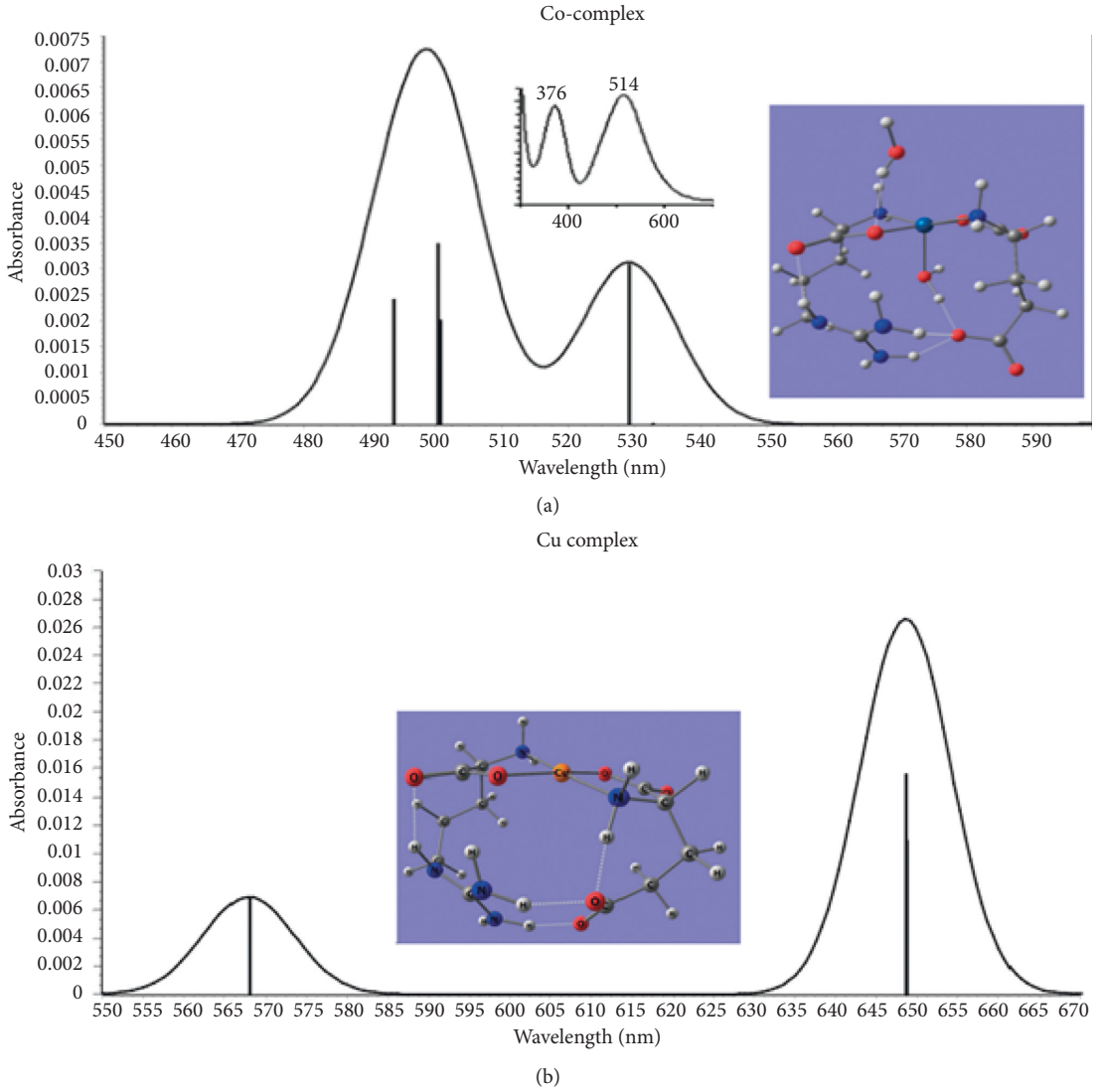

Figure 4: Theoretical and experimental (inset) UV-Vis spectra of aqueous Co and Cu complexes reflecting the excellent agreement between the results.

Table 4: Electronic spectral data, λ_{max} bands, corresponding frequencies, and assignments of all ternary metal complexes.

Complex	B (free ion)	D_q (cm^{-1})	λ_{max} (nm)	Wavenumber (cm^{-1})	Assignments	B (complex)	β	Geometry
(1)	970	1007	376 512	$\nu_3 = 26596$ $\nu_2 = 19531$	$^4T_{1g}(F) \longrightarrow {}^4A_{2g}(F)$ $^4T_{1g}(F) \longrightarrow {}^4T_{1g}(P)$	764	0.788	Tetragonal distortion pseudosquare pyramidal (distorted octahedral)
(2)	1080	894	390 632 740	$\nu_3 = 25641$ $\nu_2 = 15822$ $\nu_1 = 13586$	$^3A_2(\mathrm{F}) \longrightarrow {}^3T_1(\mathrm{P})$ $^3A_2(F) \longrightarrow {}^3T_2(F)$ $^3A_2(F) \longrightarrow {}^3T_1(F)$	765.23	0.709	Tetragonal distortion pseudosquare pyramidal (distorted octahedral)
(3)	—	1107	506 636	$\nu_2 = 19763$ $\nu_1 = 15723$	$^2B_{1g} \longrightarrow {}^2B_{2g}$ $(d_{x2-y2} \longrightarrow d_{z2})$ $^2B_{1g} \longrightarrow {}^2A_{1g}$ $(d_{x2-y2} \longrightarrow d_{xz})$	1007	—	Tetragonal distorted (square planar)
(4)	—	—	221	$\nu_1 = 45249$	Charge transfer	—	—	Tetragonal distortion pseudosquare pyramidal (distorted octahedral)

$$B_{\text{complex}} = \frac{\left(2\nu_1^2 + \nu_2^2 - 3\nu_1\nu_2\right)}{\left(15\nu_2 - 27\nu_1\right)}. \quad (4)$$

Then, $10D_q = 10637.253\ \text{cm}^{-1}$ is compared to the value of $10935\ \text{cm}^{-1}$ obtained by the first method and both values confirm octahedral structure [34]. The magnetic moment of the nickel complex was 3.1 which also confirmed octahedral structure [16].

Racah parameters for Co(II) complex is also calculated similarly.

Furthermore, Co(II) complexes have the effective magnetic moment $\mu_{\text{eff}} = 4.13$. This value is higher than spin only moment for three unpaired electrons 3.89 due to a considerable orbital contribution [34, 36].

The Zn complex did not show any d-d transitions but displayed charge transfer bands as shown in Table 4. The existence of charge transfer was due to transition between two different principle quantum numbers from three to four as distorted tetrahedron being completed by two water molecules and forms zinc octahedral complex [34–37].

The longest wavelength weak peaks are observed at 516 nm ($\varepsilon \cdot M = 20.6\ \text{L}\cdot\text{mol}^{-1}\cdot\text{cm}^{-1}$) and 636 nm ($\varepsilon \cdot M = 17.9\ \text{L}\cdot\text{mol}^{-1}\cdot\text{cm}^{-1}$) for Co(II) and Cu(II) complexes, respectively. The use of TD-DFT at BP86, DEF2-SVP, and auxiliary basis DEF2/JK level in water (using SMD solvation model) [24] results in $\lambda_{\max}$ Co = 529.1 nm (oscillator strength, $f = 0.003$) and $\lambda_{\max}$ Cu = 648.6 nm ($f = 0.0256$), which are in excellent agreement with the experimental results.

The computed natural transition orbitals of the longest wavelength transitions in both complexes reveal the largest (greater than 82%) contribution of beta HOMO-LUMO with minor (about 10.8%) contribution of alpha HOMO-LUMO in case of Co(II) complex and about 99.2% contribution from the beta-HOMO-LUMO in case of Cu(II) complex. MOs involved in the electronic transitions are depicted in Figure 5, which illustrate clear dxz or dyz $(e) \longrightarrow dz^2$ (a_1) transition in the local square pyramidal (C_{4v}) of Co(II) ion in the Co(II) complex. Metal $dxy\,(b_{2g}) - dx^2 - y^2\,(b_{1g})$ transition is dominant in case of local square planar symmetry of the Cu(II) complex. This is approved by low molar absorptivity experimentally observed in the UV-Vis spectra of both complexes and supported by low value of the computed oscillator strengths of the forbidden d-d transitions, which acquire some allowness due to geometry distortion of both complexes.

3.1.4. ESR Spectra. For elucidation of the geometry of the copper ternary complex, ESR measurement gives very useful information about the stereo chemistry bonding between copper and ligands. Figure 1S shows the ESR spectrum of the copper complex with a comparative advantage and axial symmetry (g || (parallel) = 2.10748; $g^{\perp}$ (perpendicular) = 2.01232 (=2.04984). These values confirm square planar coordination in which $g\,||\, > g^{\perp} > 2$, so the unpaired electron found in the $dx^2 - y^2$ orbital and the ground state is $^2B_{1g}$ [38]. The observed and calculated g values are different from $g_e = 2.0023$ due to spin-orbit coupling. The computed g components are not equal reflecting anisotropic effect, and the value of g changes as a function of the orientation of the molecule relative to the external magnetic field. This value is close to the spin only value, and it is in a fair agreement with the computed electron spin only value of g_e(computed) = 2.0498 [38]. Co(II) complex is characterized by $g = 2.1280$. The simulated EPR spectrum of Co(II) complex returns g_e value of 2.1085.

Different values of Mulliken spin density are shown in Figure 4S in such metal-chelates point to purely anisotropic couplings. The unpaired electron is totally localized on Co(II) ion. In case of Cu(II)-complex, electron spin population is more distributed, with about 46% on the Cu(II) ion. This may result in the simulated significant HF coupling in the case of chelating atoms around Cu(II) ion. The data point to mixed copper-nitrogen and copper-oxygen bonds in agreement with the computed optimized geometry [38].

3.2. Thermal Analysis. Thermogravimetric analysis (TGA) for the all prepared ternary metal complexes was carried out in nitrogen atmosphere. The thermal decomposition of the four complexes displayed similar patterns as their ligands.

It is well known that amino acids exist only in solid state, so their thermal decomposition has been endothermal between −72 and −151 kJ/mol when heating in range between 185°C and 280°C. Their thermal decomposition releases three gases, mainly H_2O, less NH_3, and hardly any CO_2. TGA gives the weight of these gases as weight loss calculations, which evolve in appreciable amount [39].

Also, the thermal decomposition of L-arginine-doped KDP potassium dihydrogen phosphate crystal started to lose weight with temperature from 341 K to 393 K, released ammonia and water molecules gases [40].

The amino acids are totally broken within the range 603–793K as shown in Figure 6 and Table 5. The first steps are weight loss of the three gases H_2O, NH_3, and CO_2 within temperature range about ~423–623 K. The hydrocarbons matter loses weight in the temperature range ~350–520°C. The residues for these complexes are mixture with different ratios of metal and metal oxide above temperature range 643–793 K.

It is noteworthy to mention that the geometries of the studied complexes are similar to L-arginine metal complex reported before [41], which have been confirmed by X-ray crystallographic data of single crystals.

3.3. Nanosized Metal Oxides Characterization

3.3.1. XRD of Nano CuO and Nano Cobaltosic Oxide (Co_3O_4). XRD of thermal synthesized copper oxide nanoparticles starting from copper glutamic arginine-mixed ligands complex gives characteristic peaks at 2θ 32.6°, 35.6°, 38.7°, 48.9°, 53.6°, 58.2°, 61.6°, 66.3°, and 68.1° for the marked indices of (110), (002), (111), (202), (020), (202), (113), (022), and (113), respectively, as shown in Figure 7(a) which is comparable with the literature values. The average primary particle size of the copper(II) oxide nanoparticles was

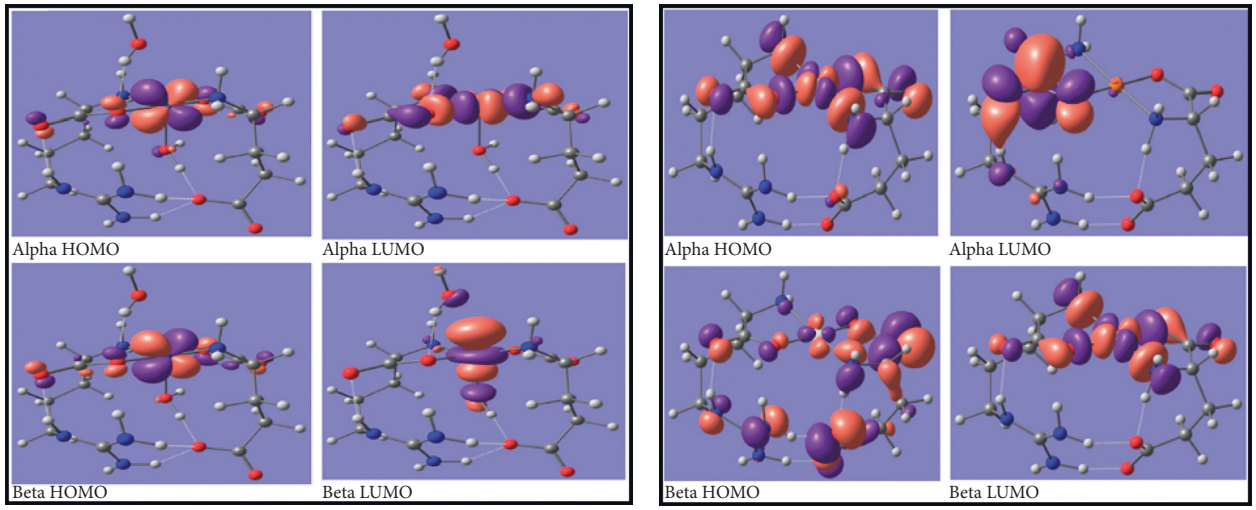

Figure 5: Frontier MOs of (a) Co(II) complex and (b) Cu(II) complex involved in the longest wavelength electronic transition. Surfaces similar to that of Co complex are obtained in case of Ni. There are no d-d transitions in Zn complexes.

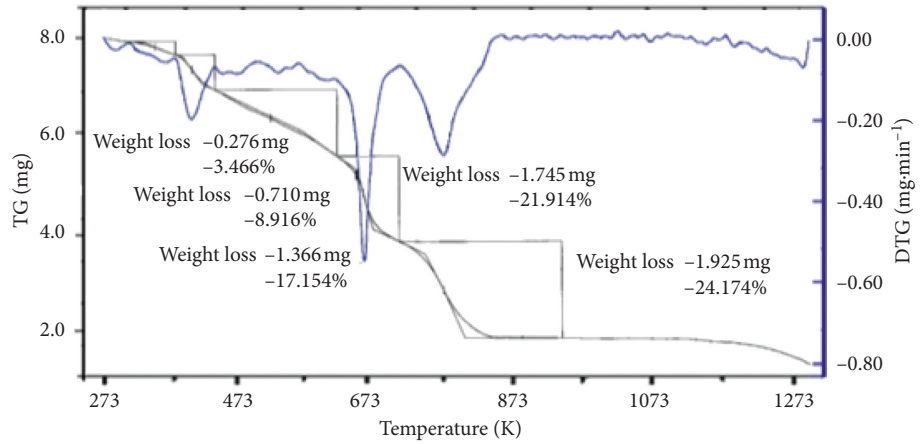

Figure 6: Continued.

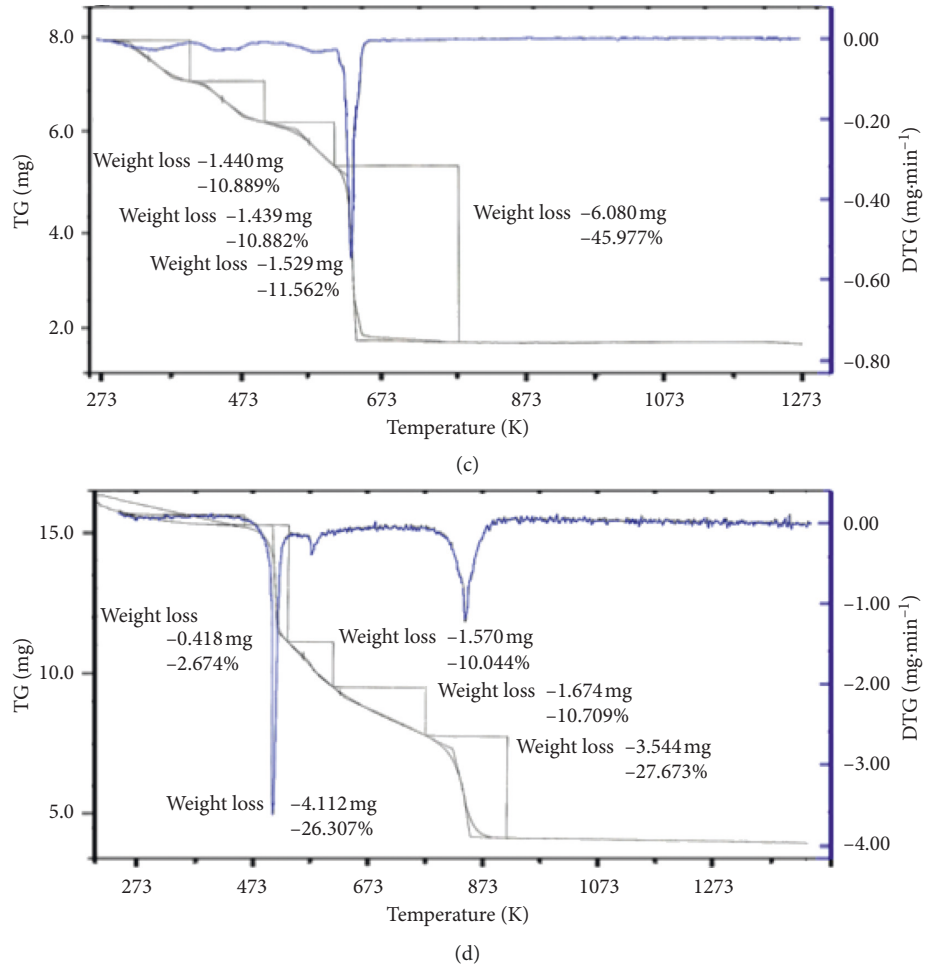

Figure 6: TG and DTG of (a) $[Co(glu)(arg)(H_2O)_2]\cdot 0.5H_2O$, (b) $[Ni(glu)(arg)(H_2O)_2]\cdot 0.5H_2O$, (c) $[Cu(glu)((arg)]\cdot H_2O$, and (d) $[Zn\cdot Glu\cdot Arg\cdot(H_2O)_2]\cdot H_2O$.

Table 5: Thermogravimetric analysis decomposition data for the metal ternary complexes.

Complexes	Mol. (wt.)	TG range (°C)	Mass loss (%) found (calculated)	Total mass loss (%)	Assignment
(1)	425.26	64.39–126.84	10.89 (10.58)	79.30	$2.5H_2O$
		170.25–224.93	10.88 (10.95)		$CO + NH_3$
		298.49–343.38	11.56 (11.99)		$3\ NH_3$
		369.82–381.85	45.97 (45.15)		Organic compound ($C_{10}H_{10}NO_3$)
		Above 381.85	20.70 (21.33)		Mix Co + CoO
(2)	425.03	78.30–124.19	14.11 (14.59)	78.61	$2.5H_2O + NH_3$
		356.95–371.58	64.51 (63.76)		Organic compound ($C_{11}N_4O_4H_{19}$)
		Above 371.58	21.38 (21.65)		Mix Ni + NiO residue
(3)	402.87	35.02–188.97	2.67 (2.23)	77.40	$0.5H_2O$
		229.63–238.11	26.31 (25.81)		$0.5H_2O + 3NH_3 + CO_2$
		284.95–294.79	10.04 (10.92)		CO_2
		294.79–332.02	10.71 (11.17)		$NH_3 + CO$
		480.35–505.88	27.67 (27.80)		Organic compound (C_8NH_2)
		Above 505.88	22.60 (22.07)		Mix Cu + CuO
(4)	440.71	80.03–112.09	3.47 (4.08)	75.62	$1H_2O$
		133.49–160.63	8.92 (8.17)		$2H_2O$
		297.44–329.5	17.15 (17.70)		$2NH_3 + CO_2$
		374.04–395.85	21.91 (21.60)		$3NH_3 + CO_2$
		468.44–522.78	24.17 (25.20)		Organic compound (C_9H_3)
		Above 522.78	24.38 (23.25)		Mix Zn + ZnO

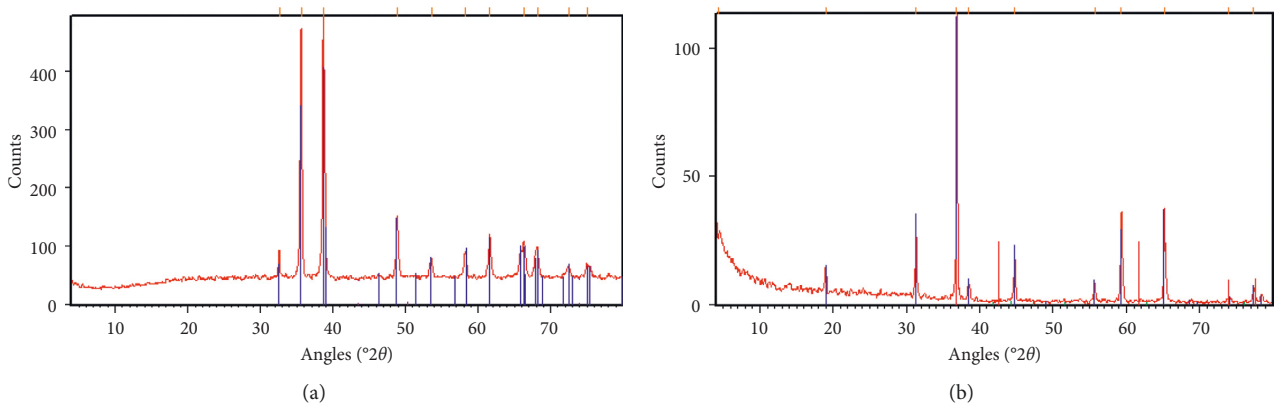

FIGURE 7: XRD pattern of (a) copper oxide, CuO, and (b) cobalt oxide, Co_3O_4, prepared by thermal decomposition at 550 C° starting from metal glutamic arginine mixed ligands complex.

estimated using well-known Debye–Scherrer formula, using the full width at half maximum (FWHM) of the (111) peaks in the XRD. K(α) is the wavelength of X-ray source (1.5406 Å = 0.15406 nm), $\beta = \Delta\theta$ is the full width at half maximum (FWHM = 0.1378), and $\theta = 38.7$ is the diffraction angle corresponding to the lattice plane (111) which gives D ~14.3–20.4 ± 0.8 nm patterns [42–44].

The pattern of XRD for cobalt oxide nanoparticles shows characteristic peaks at 2θ values at 18.98°, 31.27°, 36.82°, 38.48°, 44.78°, 55.68°, 59.34°, 65.21°, and 77.31° which are corresponding to their indices (111), (220), (311), (400), (511), and (440), in agreement with JCPDS Card No 76–1802. This pattern confirms the phase formation of cobalt oxide nanoparticle Figure 7(b). The average size of the Co_3O_4 particles was calculated by the Debye–Scherrer equation $D = K(\alpha)\,\lambda/(\beta \cos\theta)$ where D is the average crystalline size λ is the wavelength of CuKα, θ is Bragg's angle, and β is the full width at half maximum (FWHM) of the diffraction peak. The average dimension D is ~14.7–18.2 ± 0.6 nm at $2\theta = 36.82°$ which is the intense peak [44].

3.3.2. EDX of Nano CuO. The synthesized nano copper oxide is confirmed by the EDX spectrum and SEM image measurement shown in Figure 8, which confirms the highest formation percent of CuO and traces of copper carbide. The SEM image for nano copper oxide CuO shows a mixing nanosize 27.0~107.9 nm [42, 43].

3.3.3. EDX of Nano Cobaltosic Oxide. The synthesized nano cobalt oxide is confirmed by the EDX spectrum measurement shown in Figure 9, which confirms the highest formation percent of cobaltosic oxide Co_3O_4 and traces of cobalt carbide.. The SEM image for nano cobaltosic oxide Co_3O_4 shows a mixing nanosize 31.8–85.43 nm.

3.4. Applications

3.4.1. Biological Activity. Mixed ligand ternary complexes have been examined for their *in vitro* antimicrobial activity. This investigation was performed using the diffusion agar technique (Figure 5S). The assays collection included *g-negative* (*Pseudomonas aeruginosa* RCMB 010043 and *Escherichia coli* RCMB 010052) *pathogenic bacteria* using *Gentamicin* 5 mg/ml as a reference compound and *g-positive* (*Streptococcus pneumoniae* RCMB 010010 and *Bacillis subtilis* RCMB 010067) pathogenic bacteria using *Ampicillin* 5 mg/ml as a reference compound. It was also included four fungi (*Aspergillus fumigatus* RCMB 02568, *Syncephalastrum racemosum* RCMB 05922, *Geotrichum candidum* RCMB 05097, and *Candida albicans* RCMB 05036) using *Amphotericin B* 5 mg/ml as a reference compound [30, 45].

The inhibitory effects of the used ligands and their ternary polymer complexes against the used organisms are given in Table 6. In general, the used ligands did not display antifungal or antibacterial inhibitory.

For antifungal assay examination and based on the minimum inhibitory concentration (MIC) values, it is found that the inhibitory effect of all the ternary complexes vary from moderate to weak against *Amphotericin B* control except in the case of *Candida albicans* (RCMB 05036), which is not affected by both cobalt and zinc complexes.

The antibacterial activities of the obtained ternary complexes are determined in terms of MIC values. As shown in Table 6, all complexes display moderate activities against *Streptococcus pneumonia* (RCMB 010010) and *Bacillis subtilis* RCMB 010067. The growth of the gram-negative bacteria *Pseudomonas aeruginosa* RCMB 010043 and *Escherichia coli* RCMB 010052 is extremely affected by both copper and nickel complexes which display strong inhibition against the gram-negative pathogenic bacteria with MIC value less than the *Gentamicin* control. The remaining complexes do not display the same behavior during the assay.

3.4.2. Cytotoxicity. One of the fundamental goals in medicinal chemistry is the development of new anticancer and antimicrobial therapeutic agents. Cancer treatment using metal-based drugs is one of the very effective strategies as the metal ions are capable of binding to nucleic acids stereospecifically with varying strength.

In vitro anticancer activity evaluation of the newly synthesized compounds was carried out against human

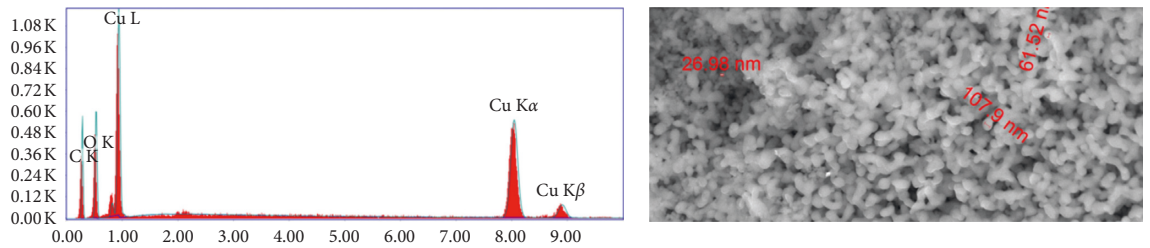

(a) (b)

Figure 8: EDX and SEM images of CuO obtained by thermal decomposition at 550 C° starting from copper glutamic arginine mixed ligands complex.

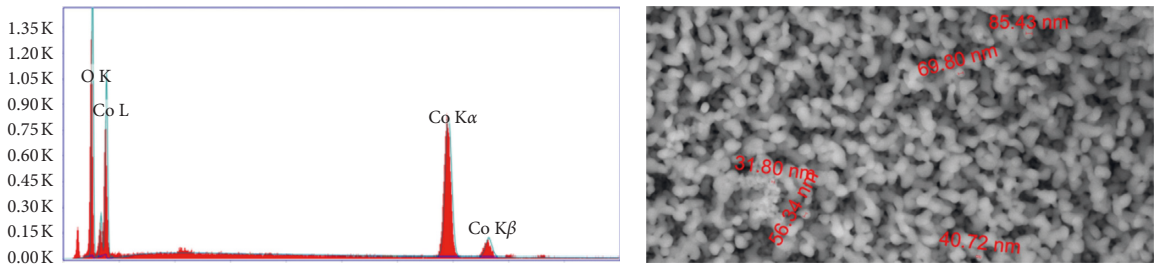

(a) (b)

Figure 9: EDX and SEM images of Co_3O_4 obtained by thermal decomposition at 550 C° starting from cobalt glutamic arginine mixed ligands complex.

Table 6: Antimicrobial activity of prepared ternary metal complexes.

Sample tested microorganisms	Glutamic acid	L-arginine	(1)	(2)	(3)	(4)	Standard
Fungi							Amphotericin B
Aspergillus fumigatus (RCMB 02568)	13.4 ± 0.63	9.3 ± 0.44	16.9 ± 0.37 (31.25)	23.2 ± 0.25 (62.5)	20.0 ± 0.58 (3.9)	16.2 ± 0.63 (62.5)	23.7 ± 0.1 (0.24)
Syncephalastrum racemosum (RCMB 05922)	15.2 ± 0.44	7.4 ± 0.63	15.6 ± 0.25 (62.5)	22.0 ± 0.58 (62.5)	14.5 ± 0.44 (12.5)	14.7 ± 0.44 (12.5)	19.7 ± 0.2 (3.9)
Geotrichum candidum (RCMB 05097)	15.9 ± 0.37	14.8 ± 0.58	17.2 ± 0.58 (31.25)	23.9 ± 0.37 (31.25)	21.2 ± 0.72 (1.95)	15.3 ± 0.44 (62.5)	28.7 ± 0.2 (0.015)
Candida albicans (RCMB 05036)	NA	NA	NA (NA)	16.2 ± 0.63 (62.5)	20.0 ± 0.17 (3.9)	NA (NA)	25.4 ± 0.1 (0.12)
Gram-positive bacteria							Ampicillin
Streptococcus pneumonia (RCMB 010010)	NA	11.9 ± 0.25	13.9 ± 0.63 (12.5)	20.3 ± 0.17 (12.5)	18.5 ± 0.44 (7.81)	20.04 ± 0.58 (3.9)	23.8 ± 0.2 (0.24)
Bacillis subtilis (RCMB 010067)	NA	14.1 ± 0.37	21.3 ± 0.44 (1.95)	22.9 ± 0.44 (3.9)	15.8 ± 0.63 (62.5)	22.08 ± 0.58 (0.98)	32.4 ± 0.3 (0.007)
Gram-negative bacteria							Gentamicin
Pseudomonas aeruginosa (RCMB 010043)	11.9 ± 0.25	NA	NA (NA)	21.4 ± 0.58 (3.9)	19.9 ± 0.44 (3.9)	12.7 ± 0.63 (12.5)	17.3 ± 0.1 (15.63)
Escherichia coli (RCMB 010052)	11.8 ± 0.63	15.2 ± 0.37	16.2 ± 0.44 (62.5)	24.8 ± 0.17 (12.5)	20.9 ± 0.58 (1.95)	18.6 ± 0.44 (7.81)	19.9 ± 0.3 (3.9)

*NA, no activity. Values in bracket are the MIC values.

cancer cell lines hepatocellular carcinoma (HePG2) because liver cancer is the third most common cause of death in cancer using MTT method [26, 46, 47].

Doxorubicin HCl is one of the most effective anti-cancer agents is used as a reference drug in this study. The obtained results from Table 2S indicated that most of these molecules' behavior can be observed from the values of the half maximal inhibitory concentration IC_{50}, which for glutamic and arginine are 16.7 and 37.6 μg/ml, respectively.

IC_{50} results indicate that the ternary complexes have promised inhibition of HePG2 liver tumors [48, 49].

Cell viability was assessed by the mitochondrial-dependent reduction of yellow MTT (3-(4,5-dimethylthiazol-2-yl)-2,5-

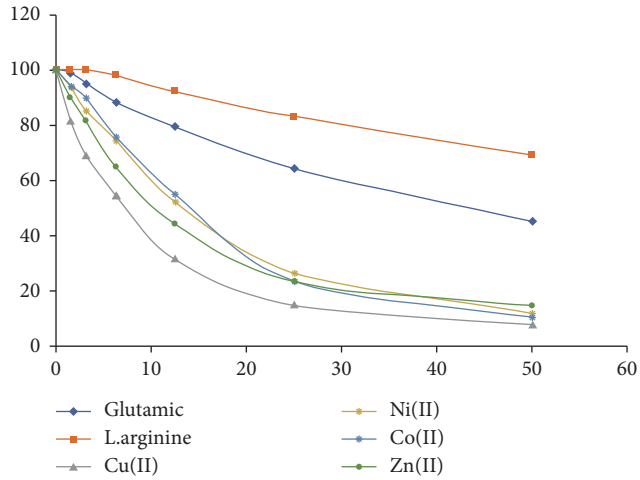

Figure 10: Cell viability of (HePG2) at different concentrations of ligands and the prepared metal complexes.

Table 7: Simulated electrical properties of complexes studied exhibiting enhanced inhibition of HePG2.

Complex	Energy (au)	HOMO (ev)	LUMO (ev)	μ (Debye)	α (A^3)	H° (au)	G° (au)	S° J/mol∗K	μ' (ev)	η (ev)
Co(II)	−2692.2	−3.713	−2.176	11.84	214.7	−2691.4	−2691.5	218	−2.94	0.77
Cu(II)	−2797.1	−5.167	−4.105	6.81	206.5	−2796.4	−2796.5	194	−4.64	0.53

diphenyl tetrazolium bromide) to insoluble purple formazan [45]. The prepared ternary metal complexes are of different viability percentages as depicted in Figure 10. Data of both ligands are also included for comparison.

Table 2S shows that the ligands have lower inhibition of HePG2 than their metal ternary complexes. The copper complex introduces the highest inhibition.

Additionally, Table 7 summarizes some computed electrical, reactivity [50], and thermodynamic properties for Co(II) and Cu(II) complexes (as maximum and minimum IC_{50} of the four prepared ternary metals complexes), which are correlated with the inhibition of human cancer cells and are useful to explain the role played by molecular properties in inhibition of human cancer cells.

The simulated data summarized in Table 7 conclude the following:

(i) Cu complex is more energetically stable relative to Co complex by about −265 kJ/mol.

(ii) Cu complex is characterized by lower dipole moment and lower polarizability relative to Co(II) complexes.

(iii) Enthalpy and Gibbs free energy of the Cu complexes are more stable by about −265 kJ/mol relative to Co(II) complex. Lower entropy reflects lower degree of randomness of Cu(II) complex.

(iv) The chemical potential (μ') (negative of molecular electronegativity) of Cu(II) complex is much higher than that of Co(II) complex reflecting the enhanced reactivity of Cu(II) complex as nucleophile because μ' measures the escaping tendency of electrons from the complex (μ' = (LUMO + HOMO)/2) [50].

(v) Cu complex is characterized by lower hardness than Co(II) complex. Hardness measures the resistance to electron transfer (η = (LUMO-HOMO)/2) [50].

It seems that more thermodynamically stable and less polar Cu complex exhibits that enhanced responsive electron cloud transfer to the surrounding tumor relative to the Co(II) complex. These quantitative molecular descriptors [50] explain the promising inhibition activity of the Cu(II) complex. The results are correlated with the above-discussed PES results, which show that Cu complex could act as nucleophile, whereas Co complex is of enhanced electrophilic nature.

The nucleophilicity of Cu complex (seeking for positively charged sites of the reactant) together with its electrical, thermodynamic, and molecular properties favors its promising inhibition activity towards HePG2 cancer cell [51–53].

3.4.3. Corrosion Inhibition of Aluminum. An assessment of corrosion rates and inhibition efficiency for aluminum with different inhibitor concentrations were computed as follows: corrosion rate R_{corr} was computed using equation (5):

$$R_{corr} = \frac{(M_1 - M_2)\,(\text{mg})}{A\,(\text{cm}^2) \times t\,(\text{h})}, \tag{5}$$

where M_1 = weight (g) before immersion, M_2 = weight (g) after immersion, A = area (cm^2) of the specimen, and t = exposure time (h).

The inhibition efficiency (%IE) was evaluated using equation (6):

$$\%\text{IE} = \left[\frac{R_{\text{blank}} - R_{\text{inh}}}{R_{\text{blank}}}\right] \times 100, \tag{6}$$

Table 8: Corrosion parameters for aluminum in aqueous solution of 1M HCl in the absence and presence of different concentrations of mixed ligands and their metal complexes at different temperatures for 7 hrs.

Inhibitors	C ($\times 10^{-2}$ M)	Corrosion rate $\times 10^{-4}$ ($g \cdot h^{-1} \cdot cm^{-2}$)			Inhibition efficiency (IE%)		
		293 K	303 K	313 K	293 K	303 K	313 K
Mixed ligand (Arg : Glu) ratio (1 : 1)	00	3.47	7.32	11.58	—	—	—
	0.01	2.60	5.93	9.73	25	19	16
	0.02	2.50	5.64	9.26	28	23	20
	0.03	2.22	5.20	8.80	36	29	24
	0.04	1.80	4.76	8.34	48	35	28
	0.05	1.60	4.39	7.76	54	40	33
	0.06	1.35	3.22	6.95	61	56	40
	0.07	1.11	3.07	6.25	68	58	46
$[Co(glu)\cdot(arg)\cdot(H_2O)_2]\cdot 0.5H_2O$	0.01	1.46	2.78	4.28	58	62	63
	0.02	1.28	2.49	3.71	63	66	68
	0.03	1.08	2.12	3.13	69	71	73
	0.04	0.97	1.76	2.90	72	76	76
	0.05	0.83	1.46	2.08	76	80	82
	0.06	0.87	1.32	1.62	75	82	86
	0.07	0.73	1.10	1.15	79	85	90
$[Ni(glu)\cdot(arg)\cdot(H_2O)_2]\cdot 0.5H_2O$	0.01	2.19	4.32	6.60	37	41	43
	0.02	2.01	4.10	6.14	42	44	47
	0.03	1.77	3.66	5.44	49	50	53
	0.04	1.53	3.22	4.98	56	56	57
	0.05	1.35	2.71	3.94	61	63	66
	0.06	1.15	2.27	3.47	67	69	70
	0.07	0.97	2.05	2.90	72	72	75
$[Cu(glu)\cdot((arg)]\cdot H_2O$	0.01	2.32	4.76	7.18	33	35	38
	0.02	2.12	4.25	6.25	39	42	46
	0.03	1.91	3.88	5.91	45	47	49
	0.04	1.63	3.37	5.21	53	54	55
	0.05	1.46	3.07	4.86	58	58	58
	0.06	1.32	2.71	4.05	62	63	65
	0.07	1.18	2.34	3.47	66	68	70
$[Zn(glu)\cdot(arg)\cdot(H_2O)_2]\cdot H_2O$	0.01	1.25	2.42	3.59	64	67	69
	0.02	1.08	2.05	3.13	69	72	73
	0.03	0.83	1.61	2.43	76	78	79
	0.04	0.73	1.54	2.08	79	79	82
	0.05	0.62	1.17	1.74	82	84	85
	0.06	0.59	0.95	1.39	83	87	88
	0.07	0.52	0.81	0.93	85	89	92

where R_{blank} = corrosion rates in the absence of inhibitor and R_{inh} = corrosion rates in the presence of inhibitor [16].

Table 8 shows the calculated corrosion rates and inhibition efficiencies of aluminum specimens in aqueous solution of 1M HCl as the corrosive medium in absence and presence of mixed ligands and their ternary metal complexes at different temperatures (293 –313) K for 7 hours of each concentration. Figure 6S shows that, as the concentration of ligands and their complexes increases, R_{corr} decreases and %IE increases for mixed ligands, and their metal complexes acted as more efficient inhibitors than their mixed ligands alone.

3.4.4. Adsorption Isotherms and the Thermodynamic Activation Parameters. The metal surface coverage degree (θ = %IE/100) was subjected to different adsorption isotherms. The well fit for weight loss data is obtained for Langmuir adsorption isotherm Figure 11.

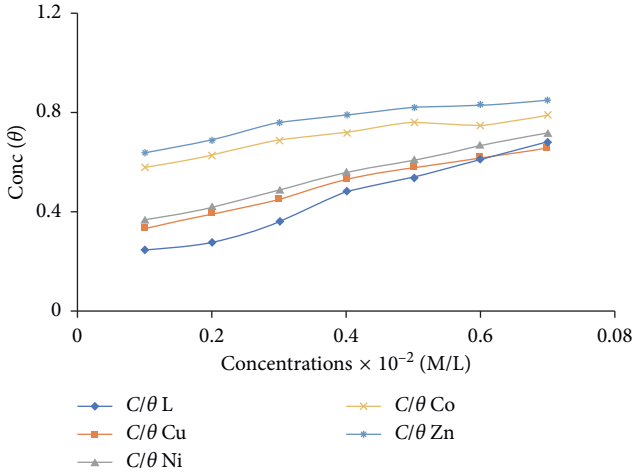

Figure 11: Langmuir adsorption isotherms of the mixed ligands (L) and their metal complexes.

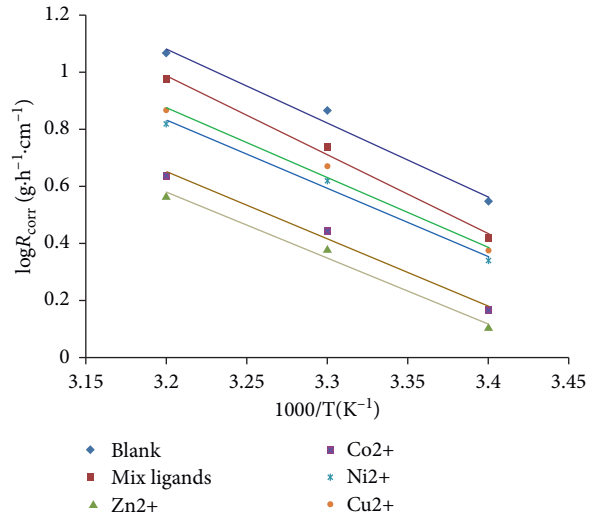

FIGURE 12: Arrhenius of log corrosion rate (R_{corr}) vs $1/T$ for aluminum in 1M HCl without and with 0.04×10^{-2} ML^{-1} of inhibitors (mixed ligands and their metal complexes).

TABLE 9: Thermodynamic parameters for the adsorption of (0.04×10^{-2}) M/L mixed ligands and their metal complexes on aluminum metal in aqueous solution of 1 M HCl at different temperatures for 7 hrs.

Compound	Temp. (K)	Corrosion rate $\times 10^{-4}$ (g·h^{-1}·cm^{-2})	IE %	E_a^* (kJ·mol^{-1})	ΔH^* (kJ·mol^{-1})	ΔG^* (kJ·mol^{-1})	ΔS^* (kJ·mol^{-1}·K^{-1})
Blank	293	3.47	—	66.002	47.556	52.080	−0.0149
	303	7.32	—				
	313	11.58	—				
Mixed ligand (Arg: Glu) ratio (1 : 1)	293	1.8	48	69.528	61.191	53.268	0.0262
	303	4.76	35				
	313	8.34	28				
(1)	293	0.97	72	58.822	46.517	54.165	−0.0252
	303	1.76	76				
	313	2.90	76				
(2)	293	1.53	56	60.459	43.025	55.510	−0.0412
	303	3.22	56				
	313	4.98	57				
(3)	293	1.63	53	61.845	41.030	56.139	−0.0499
	303	3.37	54				
	313	5.21	55				
(4)	293	0.73	79	57.688	45.810	54.035	−0.0271
	303	1.54	79				
	313	2.08	82				

The temperature effect (293–313 K) on aluminum weight loss inhibition may be attributed to two main mechanisms: physical and chemical adsorption [37]. The suggested mechanisms are obtained as the temperature increases, the efficiency decreases for mixed ligands but increases for their metal complexes depending on the nature of bond formation between the mixed ligands and aluminum surface, which is different from the nature of bond formation between metal complexes and the aluminum surface [16]. Arrhenius equation (7) gives the relation between the corrosion rate and temperature:

$$\ln R_{corr} = \ln A - \frac{E^*}{RT}, \tag{7}$$

where A is the Arrhenius factor, E^* is the apparent activation energy of the corrosion process, R is the rate gas constant, and T is the absolute temperature. The straight line slope of $\log R_{corr}$ vs $1/T$ for aluminum 1 M HCl at 4×10^{-4} mol/L after 7 h is $-E^*/2.303R$ for the inhibitors (Figure 12).

The activation thermodynamic parameters for aluminum dissolution could be obtained from the transition state equation (8):

$$\ln\left(\frac{R_{corr}}{T}\right) = \ln\left(\frac{R}{Nh}\right) + \left(\frac{\Delta S^*}{R}\right) - \left(\frac{\Delta H^*}{RT}\right), \tag{8}$$

where the entropy of activation ΔS^* and the apparent enthalpy of activation ΔH^* can be obtained from the intercept

and the slope for the straight line of the relation between $\ln(R_{corr}/T)$ vs $(1/T)$, respectively. N is Avogadro's number, and h is Planck's constant. The Gibbs free energy of activation ΔG^* can be detected by equation (9):

$$\Delta G^* = \Delta H^* - T\Delta S^*. \quad (9)$$

Table 9 shows the thermodynamic parameters for the adsorption of mixed ligands and their metal complexes. The positive value of ΔH^* indicated the endothermic property of dissolution process nature for aluminum in the acidic medium [54].

However, the blank ΔH^* value is higher than the inhibitor metal complexes, which indicated that the inhibition efficiency generally increases with increasing temperature. The association step is the rate-determining step rather than a dissociation process in presence of the metal complexes inhibitors due to the negative values of ΔS^*. It is known that the values of ΔG^* above 40 kJ·mol^{-1} are referred to charge transfer from the inhibitor molecules into aluminum surface to form coordinated compound on the Al surface which blocks it against corrosion process by different degrees. Also, the chemical adsorption process mechanism is confirmed by the values of ΔG^* above 40 kJ·mol^{-1} [16, 54–56].

4. Conclusions

Novel coordination materials of ternary divalent metal ions (Cu(II), Ni(II), Co(II), and Zn(II)) chelated by the bidentate glutamic acid (Glu) and L-arginine (Arg) amino acids are synthesized and characterized. The metal ions complexes are modelled using density DFT and TD-DFT theory. Computed molecular and spectroscopic (IR, UV-Vis, and EPR) properties validated the experimental results. The used computational methods are capable of providing good structural descriptions for the TM complexes. Consistent with the experimental properties, the optimized structures of the complexes [Cu(II) Glu-Arg] and [Co(II) Glu-Arg $(H_2O)_2$] reveal that symmetry environment of Cu(II) exhibits slightly distorted square planar shape, whereas Co(II)-complex has a distorted octahedral (where Co(II) central ion is of C_{4v}-local symmetry). Spectral properties of [Ni(II) Glu-Arg $(H_2O)_2$] and [Zn·Glu·Arg·$(H_2O)_2$] complexes indicate that they have similar structure as Co(II) complex. All the studied ternary metal complexes are of different antifungal activities ranging from moderate to weak without practically noticed inhibitory effects, whereas antibacterial activities of all studied metal complexes show significant effects.

Cytotoxicity studies against (HePG2) reveal the promising potentiality of Cu(II) complex as inhibitor of cancer cells. The results are correlated with the computed molecular descriptors including dipole moment, polarizability, thermodynamics, and reactivity properties as well as the PES maps.

The corrosion inhibition of aluminum metal specimens in 1M HCl is efficiently achieved by mixed ligands and their metal complexes studied.

Data Availability

The data used to support the findings of this study are available from the corresponding author upon request.

Conflicts of Interest

The authors declare that they have no conflicts of interest.

Supplementary Materials

The supplementary materials consist of six figures and two tables to further clarify the structures and trends of the newly prepared metal ternary complexes. (*Supplementary Materials*)

References

[1] Z. Ozturk, D. A. Kose, A. Asan et al., "Porous metal-organic Cu(II) complex of L-Arginine; 2synthesis, characterization, hydrogen storage properties and molecular simulation calculations," *Hittite Journal of Science and Engineering*, vol. 1, no. 1, pp. 1–5, 2014.

[2] S. A. Lahsasni, R. A. Ammar, M. F. Amin et al., "Mixed-ligand complex formation of Cu(II) with 1,2- diphenylethylenediamine as primary ligand and amino acids as secondary ligands," *International Journal of Electrochemical Science*, vol. 7, pp. 7699–7711, 2012.

[3] H. Sigel, B. P. Operschall, S. S. Massoud, B. Song, and R. Griesser, "Evidence for intramolecular aromatic-ring stacking in the physiological pH range of the monodeprotonated xanthine residue in mixed-ligand complexes containing xanthosinate 5′-monophosphate (XMP)," *Dalton Transactions*, vol. 46, no. 46, pp. 5521–5529, 2006.

[4] S. Udhayakumar, K. G. Shankar, S. Sowndarya, S. Venkatesh, C. Muralidharan, and C. Rose, "l-Arginine intercedes biocrosslinking of a collagen-chitosan 3D-hybrid scaffold for tissue engineering and regeneration: in silico, in vitro, and in vivo studies," *RSC Advances*, vol. 7, no. 40, pp. 25070–25088, 2017.

[5] P. K. Datta, M. Chandra, and A. K. Dey, "Ternary complexes of copper(II), nickel(II) and zinc(II) with nitrilotriacetic acid as a primary ligand and some phenolic acids as secondary ligands," *Transition Metal Chemistry*, vol. 5, no. 1–3, 1980.

[6] J. S. Woertink, L. Tian, D. Maiti et al., "Spectroscopic and computational studies of an end-on bound superoxo-Cu(II) complex: geometric and electronic factors that determine the ground state," *Inorganic Chemistry*, vol. 49, no. 20, pp. 9450–9459, 2010.

[7] S. Dutta, S. Ray, K. Nagarajan et al., "Glutamic acid analogues used as potent anticancer: a review," *Der Pharma Chemica*, vol. 3, no. 2, pp. 263–272, 2011.

[8] T. Sismanoglu, S. Pura, and A. Bastug, "Binary and ternary metal complexes of Congo red with amino acids," *Dyes and Pigments*, vol. 70, no. 2, pp. 136–142, 2006.

[9] R. N. Patel, H. C. Pandey, K. B. Pandeya et al., "Mixed ligand complex formation of nickel(II),copper(II) and zinc(II) with some amino acids and imidazoles," *Indian Journal of Chemistry-Section A Inorganic, Physical, Theoretical and Analytical Chemistry*, vol. 38, no. 8, pp. 850–853, 1999.

[10] L. Meng and Z. Lin, "Complexations of alkali/alkaline earth metal cations with gaseous glutamic acid," *Computational and Theoretical Chemistry*, vol. 1039, pp. 1–10, 2014.

[11] L. D. Pinto, P. A. L. Puppin, V. M. Behring, O. C. Alves, N. A. Rey, and J. Felcman, "Solution and solid state study of copper(II) ternary complexes containing amino acids of interest for brain biochemistry-2: homocysteine with aspartate, glutamate or methionine," *Inorganica Chimica Acta*, vol. 386, pp. 60–67, 2012.

[12] A. Wojciechowska, A. Ggor, and W. Zierkiewicz, "Chiral octahedral complexes of Co(III) as catalysts for asymmetric epoxidation of chalcones under phase transfer conditions," *RSC Advances*, vol. 5, no. 46, pp. 36295–36306, 2015.

[13] B. M. Weckhuysen, A. A. Verberckmoes, L. Fu, and R. A. Schoonheydt, "Zeolite-encapsulated copper(II) amino acid complexes: synthesis, spectroscopy, and catalysis," *Journal of Physical Chemistry*, vol. 100, no. 22, pp. 9456–9461, 1996.

[14] K. Y. El-Baradie, N. A. El-Wakiel, and H. A. El-Ghamry, "Synthesis, characterization and corrosion inhibition in acid medium ofl-histidine Schiff base complexes," *Applied Organometallic Chemistry*, vol. 29, no. 3, pp. 117–125, 2015.

[15] S. S. R. Anthony and R. Susai, "Inhibition of corrosion of carbon steel in well water by arginine-Zn^{2+} system," *Journal of Electrochemical Science and Engineering*, vol. 2, no. 2, pp. 91–104, 2012.

[16] E. H. Isamil, F. F. AlBlewi, N. Soliman, and M. M. H. Khalil, "Thermal studies and mass loss inhibition for some new mixed amino acid metal complexes with their applications," *Journal of Thermal Analysis and Calorimetry*, vol. 125, no. 1, pp. 289–300, 2016.

[17] F. Neese, "The ORCA program system 4.0.1.2.," *Wiley Interdisciplinary Reviews: Computational Molecular Science*, vol. 2, no. 1, pp. 73–78, 2012.

[18] S. Grimme, S. Ehrlich, and L. Goerigk, "Effect of the damping function in dispersion corrected density functional theory," *Journal of Computational Chemistry*, vol. 32, no. 7, pp. 1456–1465, 2011.

[19] S. Grimme, J. Antony, S. Ehrlich, and H. Krieg, "A consistent and accurate ab initio parametrization of density functional dispersion correction (DFT-D) for the 94 elements H-Pu," *The Journal of Chemical Physics*, vol. 132, no. 15, article 154104, 2010.

[20] F. Weigend, "Hartree-Fock exchange fitting basis sets for H to Rn," *Journal of Computational Chemistry*, vol. 29, no. 2, pp. 167–175, 2008.

[21] F. Neese, F. Wennmohs, and A. Hansen, "Efficient, approximate and parallel Hartree-Fock and hybrid DFT calculations A 'chain-of-spheres' algorithm for the Hartree-Fock exchange," *Chemical Physics*, vol. 356, no. 1–3, pp. 98–109, 2009.

[22] R. Izsák and F. Neese, "An overlap fitted chain of spheres exchange method," *Journal of Chemical Physics*, vol. 135, no. 14, article 144105, 2011.

[23] T. Petrenko, S. Kossmann, and F. Neese, "Efficient time-dependent density functional theory approximations for hybrid density functionals: analytical gradients and parallelization," *Journal of Chemical Physics*, vol. 134, no. 5, article 054116, 2011.

[24] A. V. Marenich, C. J. Cramer, and D. G. Truhlar, "Universal solvation model based on solute electron density and on a continuum model of the solvent defined by the bulk dielectric constant and atomic surface tensions," *Journal of Physical Chemistry B*, vol. 113, no. 18, pp. 6378–96, 2009.

[25] S. Donovan, C. Stiefbold, and K. Sprague, "Chapter 3, Chemical properties of amino acids and identification of unknown amino acids," in *Proceedings of the 17 th Workshop/Conference of the Association for Biology Laboratory Education (ABLE)*, vol. 17, pp. 35–70, Bainbridge, GA, USA, March 1996.

[26] C. C. Wagner, J. Enrique, and C. Claudia, "Vibrational and magnetic properties of a Cu/Mg glutamate complex," *Argentina Acta Farm Bonaerense*, vol. 22, no. 2, pp. 137–142, 2003.

[27] M. Arif, R. Sur, and M. Arshad, "Studies on the thermal decomposition of copper (II) flouride complexes with various amino acids in nitrogen atmosphere," *Turkish Journal of Chemistry*, vol. 25, pp. 73–79, 2001.

[28] A. Ghosh, M. J. Tucker, and R. M. Hochstrasser, "Identification of arginine residues in peptides by 2d-IR echo spectroscopy," *Journal of Physical Chemistry A*, vol. 115, no. 34, pp. 9731–9738, 2011.

[29] K. Nakamoto, *Infrared Spectra of Inorganic and Coordination Compounds Part B*, Wiley-Interscience, New York, NY, USA, 5th edition, 1997.

[30] E. Santi, M. H. Torre, E. Kremer, S. B. Etcheverry, and E. J. Baran, "Vibrational spectra of the copper(II) and nickel(II) complexes of piroxicam," *Vibrational Spectroscopy*, vol. 5, no. 3, pp. 285–293, 1993.

[31] H. N. Aliyu and A. S. Mohammed, "Synthesis, spectrophotometric and biological activity of nickel (II) and copper (II) complexes with schiff base derived from acetylacetone and histidine," *Global Advanced Research Journal of Microbiology*, vol. 1, no. 5, pp. 67–71, 2012.

[32] J. S. Murray and P. Politzer, "The electrostatic potential: an overview," *Wiley Interdisciplinary Reviews: Computational Molecular Science*, vol. 1, no. 2, pp. 153–163, 2011.

[33] E. R. Souaya, M. M. H. Khalil, and E. H. Ismail, "Synthesis and characterization of ternary complexes of certain hydroxyl acids and their biological applications," *Research Journal of Pharmaceutical, Biological and Chemical Sciences*, vol. 5, no. 4, pp. 18–30, 2014.

[34] N. N. Greenwood and A. Earnshaw, *A Review of: Chemistry of the Elements*, Pergamon Press, Oxford, UK, 1984.

[35] V. Reddy, N. Patil, and S. D. Angadi, "Synthesis, characterization and antimicrobial activity of Cu(II), Co(II) and Ni(II) complexes with O,N, and S Donor ligands," *E-Journal of Chemistry*, vol. 5, no. 3, pp. 577–583, 2008.

[36] F. A. Cotton, G. Wilkinson, C. A. Murillo et al., *Advances in Schiff Base Chemistry*, Wiley, New York, NY, USA, 6th edition, 1999.

[37] M. M. H. Khalil, E. H. Ismail, S. A. Azim, and E. R. Souaya, "Synthesis, characterization, and thermal analysis of ternary complexes of nitrilotriacetic acid and alanine or phenylalanine with some transition metals," *Journal of Thermal Analysis and Calorimetry*, vol. 101, no. 1, pp. 129–135, 2010.

[38] F. Mabbs and D. Colisson, *Electron Paramagnetic Resonance of D Transition Metal Compounds*, Vol. 102, Elsevier, Amsterdam, Netherlands, 1992.

[39] M. M. H. Khalil, E. R. Souaya, E. H. Ismail et al., "Ternary transition metal complexes of nitrilotriacetic acid and valine or leucine: synthesis and biological applications," *Chinese Journal of Inorganic Chemistry*, vol. 29, no. 9, pp. 1969–1978, 2013.

[40] I. M. Weiss, C. Muth, R. Drumm, and H. O. K. Kirchner, "Thermal decomposition of the amino acids glycine, cysteine, aspartic acid, asparagine, glutamic acid, glutamine, arginine and histidine," *BMC Biophysics*, vol. 11, no. 1, 2018.

[41] A. M. Petrosyan, V. V. Ghazaryan, G. Giester, and M. Fleck, "Sulfamates and methanesulfonates of L-arginine and L-histidine," *Journal of Molecular Structure*, vol. 1163, pp. 114–127, 2018.

[42] T. Kavitha, S. Haider, T. Kamal, and M. Ul-Islam, "Thermal decomposition of metal complex precursor as route to the synthesis of Co3O4 nanoparticles: antibacterial activity and mechanism," *Journal of Alloys and Compounds*, vol. 704, pp. 296–302, 2017.

[43] E. M. M. Ibrahim, L. H. Abdel-Rahman, A. M. Abu-Dief, A. Elshafaie, S. K. Hamdan, and A. M. Ahmed, "The synthesis of CuO and NiO nanoparticles by facile thermal decomposition of metal-Schiff base complexes and an examination of their electric, thermoelectric and magnetic Properties," *Materials Research Bulletin*, vol. 107, pp. 492–497, 2018.

[44] S. Farhadi, M. Javanmard, and G. Nadri, "Characterization of cobalt oxide nanoparticles prepared by the thermal decomposition," *Acta Chimica Slovenica*, vol. 63, pp. 335–343, 2016.

[45] E. M. Zayed, E. H. Ismail, G. G. Mohamed, M. M. H. Khalil, and A. B. Kamel, "Synthesis, spectroscopic and structural characterization, and antimicrobial studies of metal complexes of a new hexadentate Schiff base ligand. Spectrophotometric determination of Fe(III) in water samples using a recovery test," *Monatshefte für Chemie-Chemical Monthly*, vol. 145, no. 5, pp. 755–765, 2014.

[46] V. Milacic, D. Chen, L. Ronconi, K. R. Landis-Piwowar, D. Fregona, and Q. P. Dou, "A novel anticancer gold(III) dithiocarbamate compound inhibits the activity of a purified 20S proteasome and 26S proteasome in human breast cancer cell cultures and xenografts," *Cancer Research*, vol. 66, no. 21, pp. 10478–10486, 2006.

[47] T. Mosmann, "Rapid colorimetric assay for cellular growth and survival: application to proliferation and cytotoxicity assays," *Journal of Immunological Methods*, vol. 65, no. 1-2, pp. 55–63, 1983.

[48] R. L. Siegel, K. D. Miller, and A. Jemal, "Cancer statistics, 2018," *CA: A Cancer Journal for Clinicians*, vol. 68, no. 1, pp. 7–30, 2018.

[49] S. Chattopadhyay, S. P. Chakraborty, D. Laha et al., "Surface-modified cobalt oxide nanoparticles: new opportunities for anti-cancer drug development," *Cancer Nanotechnol*, vol. 3, no. 1-6, pp. 13–23, 2012.

[50] F. Zielinski, V. Tognetti, and L. Joubert, "Condensed descriptors for reactivity: a methodological study," *Chemical Physics Letters*, vol. 527, pp. 67–72, 2012.

[51] H. Wang, Y. He, Q. Yan et al., "Correlation between the dielectric properties and biological activities of human ex vivo hepatic tissue," *Physics in Medicine and Biology*, vol. 60, no. 6, pp. 2603–2617, 2015.

[52] F. Tao, F. Fu, F. You et al., "The correlation between dielectric properties and microstructure of femoral bone in rats with different bone qualities," *Annals of Biomedical Engineering*, vol. 42, no. 6, pp. 1238–1249, 2014.

[53] L. Gun, D. Ning, and Z. Liang, "Effective permittivity of biological tissue: comparison of theoretical model and experiment," *Mathematical Problems in Engineering*, vol. 2017, Article ID 7249672, 2017.

[54] E. I. Ating, S. A. Umoren, I. I. Udousoro, E. E. Ebenso, and A. P. Udoh, "Leaves extract of *Ananas sativumas* green corrosion inhibitor for aluminium in hydrochloric acid solutions," *Green Chemistry Letters and Reviews*, vol. 3, no. 2, pp. 61–68, 2010.

[55] E. Hamed, "Studies of the corrosion inhibition of copper in Na2SO4 solution using polarization and electrochemical impedance spectroscopy," *Materials Chemistry and Physics*, vol. 121, no. 1-2, pp. 70–76, 2010.

[56] H. Zarrok, H. Oudda, A. Zarrouk et al., "Weight loss measurement and theoretical study of new pyridazine compound as corrosion inhibitor for C38 steel in hydrochloric acid solution," *Der Pharma Chemica*, vol. 3, no. 6, pp. 576–590, 2011.